ORIGINAL ARTICLE

SU2 Conference 2020, 10-12 June 2020

Shape Optimization for a Conjugate- and Radiative- Heat Transfer model with turbulent fluid flows and participating media

Nicolas Dietrich[1*] | Thomas Marx[1*] | René Pinnau[1] | Emre Özkaya[2] | Rubén Fernández[2] | Nicolas Gauger[2] | Ole Burghardt[2]

[1]Mathematics, TU Kaiserslautern, 67663 Kaiserslautern, Rheinland-Pfalz, Germany

[2]Scientific Computing, TU Kaiserslautern, 67663 Kaiserslautern, Rheinland-Pfalz, Germany

Correspondence
Nicolas Dietrich, Mathematics, TU Kaiserslautern, 67663 Kaiserslautern, Rheinland-Pfalz, Germany
Email: ndietric@mathematik.uni-kl.de

Funding information
German Federal Ministry of Education and Research (BMBF), Grant Number: 05M18UKA

We present an industrial shape design optimization problem in high temperature processes based on a novel approach to compute adjoint sensitivities accurately and efficiently in a multizone and multiphysics framework involving incompressible turbulent flows, radiation, and conjugate heat transfer between a solid domain and a buoyancy-driven cavity. We verify and validate the accuracy of the shape sensitivities by a finite difference approach and demonstrate the feasibility of the method by optimizing a benchmark problem via a steepest descent gradient-based algorithm.

KEYWORDS
Shape Optimization, Coupled Adjoints, Computational Fluid Dynamics, Radiative Heat Transfer, Conjugate Heat Transfer, Multizone Problem, Multiphysics Problem

1 | INTRODUCTION

High temperature processes have a vast field of industrial application, e.g. combustion chambers, furnaces and cooling in glass industry to name some [1, 2, 3, 4, 5]. The magnitude of the temperature yields a considerable contribution of

[*]Equally contributing authors.

radiation processes by Stefans law, since the radiant flux P in a black body is proportional to the medium temperature T by the power of 4, i.e. $P \propto T^4$. Hence, we have to consider a sophisticated model for the description of Radiative Heat Transfer, which is given by the Radiative Heat Transfer Equation (RHTE) being an integro-differential equation which depends on space, time, angle, direction and frequency of the rays. For an introduction to different analytical and numerical approaches to solve this kinetic equation we refer to [6, 7, 8, 9].

For application purposes, we consider a multizone and multiphysics model, i.e., a coupling between radiation, turbulent induced air flow and conjugate heat flow between a solid and the medium.

In a second step, we want to maximize the heat flux in the solid. For that we optimize the geometry w.r.t. the multiphysics model and we are hereby interested in a consistent and efficient application of optimization procedures, coming from several disciplines such as radiation [10, 11] and aircraft design [12, 13, 14].

This Optimal Design Problem (ODP) is computationally expensive because of the coupled equations as well as the high-dimensionality of the phase space. We are going to approach this problem by a "discretize first and then optimize" approach and compute shape sensitivities using SU2, which we use as gradient information for a steepest descent method. We obtain the derivative efficiently by using algorithmic differentiation for as many design variables as desired.

We avoid computing the exact Jacobians of the problem, as this requirement is particularly complicated to meet in multidisciplinary problems. Instead we use an efficient methodology to overcome this issue, and compute accurate adjoint sensitivities in a more general framework. Previous works by Albring *et al.* [15, 16], Zhou *et al.* [17, 18], Economon [19] or Sanchez *et al.* [20, 21] have shown the applicability of these techniques for problems in turbulent fluid mechanics, aeroacoustics and low speed flows. The proposed methodology is implemented in SU2 [22, 23, 24] and we use a python script for the optimization loop, in which we call the state and adjoint solver as well as calculate the shape sensitivities w.r.t the design parameters.

This work is organized as follows: First, we introduce the multi-zone and multiphysics model of choice for the primal (physical) problem in Section 2. Second, we compute the adjoints based on AD for the multizone coupled CFD-RHT-CHT problem in Section 3. Then, we demonstrate the accuracy of the proposed adjoint method in Section 4, comparing the obtained gradients with those obtained via finite differences. Next we apply the shape gradient information in a benchmark shape design optimization problem in Section 4.2 to underline the feasibility of the approach. In the last Section 5 we give conclusions and discuss future research topics.

2 | PRIMAL PROBLEM

We consider a multiphysics multizone problem in which the the primal (physical) problem is given on the two subdomains shown in Figure 1. In zone 1 a buoyancy-driven cavity transports heat throughout the domain and interacts with the solid in zone 2. This is modeled by three coupled subproblems. The Navier-Stokes equations for turbulent flows, introduced in Section 2.1), is coupled with the P1 approximation of the Radiative Heat Transfer Equation, introduced in Section 2.2. The heat transfer between the fluid and the solid body is modeled via Conjugate Heat Transfer. The heat equation is explained in Section 2.3 and the coupling conditions between the three solvers, which are needed for a segregated implementation, are introduced in Section 2.4

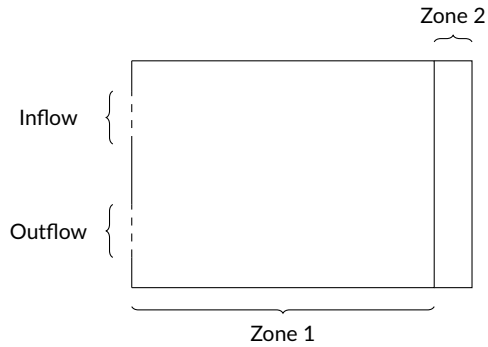

FIGURE 1 A possible benchmark geometry with zone 1, where the Navier-Stokes and P1 system governs and zone 2, which is a solid where the conjugate heat transfer governs

2.1 | Fluid mechanics

As fluid dynamical model, we consider first turbulent flows in an ideal gas situation governed by the Navier-Stokes equations with energy equation. As a flow solver we use the incompressible one from SU2 [24].

We may write the governing equations in their residual form as:

$$F(\mathbf{w}) = \frac{\partial \mathbf{w}}{\partial t} + \nabla \cdot \mathbf{F}^c(\mathbf{w}) - \nabla \cdot \mathbf{F}^v(\mathbf{w}) - \mathbf{Q}(\mathbf{w}) = 0, \tag{1}$$

where $\mathbf{w} = (\rho, \rho\mathbf{v}, \rho c_p T)$ is the vector of conservative variables, ρ the flow density, $\mathbf{v}$ the flow velocity, c_p the specific heat at constant pressure, and T the flow temperature. $\mathbf{F}^c(\mathbf{w})$ and $\mathbf{F}^v(\mathbf{w})$ are, respectively, the convective and viscous fluxes, which can be written as

$$\mathbf{F}^c(\mathbf{w}) = \begin{pmatrix} \rho\mathbf{v} \\ \rho\mathbf{v} \otimes \mathbf{v} + \rho\mathbf{I} \\ \rho c_p T \mathbf{v} \end{pmatrix}, \quad \mathbf{F}^v(\mathbf{w}) = \begin{pmatrix} \cdot \\ \boldsymbol{\tau} \\ \kappa \nabla T \end{pmatrix}, \tag{2}$$

and $\mathbf{Q}$ is a source term, which for a body force $\mathbf{f}$ can be written as

$$\mathbf{Q}(\mathbf{w}) = \begin{pmatrix} \cdot \\ \rho\mathbf{f} \\ \cdot \end{pmatrix}. \tag{3}$$

As is usually done, we rewrite Equation 1 in terms of the primitive variables $\mathbf{q} = (p, \mathbf{v}, T)$ and precondition the time term to get

$$F(\mathbf{q}) = \Gamma(\beta)\frac{\partial \mathbf{q}}{\partial t} + \nabla \cdot \mathbf{F}^c(\mathbf{q}) - \nabla \cdot \mathbf{F}^v(\mathbf{q}) - \mathbf{Q}(\mathbf{q}) = 0, \tag{4}$$

where $\Gamma(\beta)$ is a preconditioning matrix and β is a preconditioning factor. The steady version of this Equation is solved in SU2 using an implicit Euler scheme. Details can be found in the respective configurations, see Section 4.

2.2 | Radiative Transfer Equation

The unsteady, frequency dependent Radiative Transfer Equation in participating media is given by the following integro-differential equation

$$\begin{aligned}\frac{1}{c}\frac{\partial I(\mathbf{u},t,\mathbf{\Omega})}{\partial t} + \mathbf{\Omega}\cdot\nabla I(\mathbf{u},t,\mathbf{\Omega}) &= \kappa\left[I_b(\mathbf{u},t) - I(\mathbf{u},t,\mathbf{\Omega})\right] \\ &+ \sigma_s\left[\int_s g(\mathbf{\Omega}\cdot\mathbf{\Omega}')I(\mathbf{u},t,\mathbf{\Omega}')d\mathbf{\Omega}' - I(\mathbf{u},t,\mathbf{\Omega})\right],\end{aligned} \tag{5}$$

where $\mathbf{u}$ is the space coordinate, $t > 0$ the time and $\mathbf{\Omega}$ the solid angles covered by the rays. Further, $I(\mathbf{u},t,\mathbf{\Omega},\nu)$ is the radiation intensity at $(\mathbf{u},t)$ pointing in direction $\mathbf{\Omega}$ with frequency ν, $I_b(\mathbf{u},t,\nu)$ is the blackbody radiation intensity, κ is the absorption- and σ_s is the scattering coefficient. The direct integration of Equation (5) can be done by a finite volume method or the so-called discrete ordinates method (DOM) [25, 26, 27, 28, 29], but these numerical approaches are computationally expensive. Instead, we are simplifying the problem by considering media of gray matter, i.e., we do not need to take into account frequency dependencies and we consider the steady case, since we are not interested in the warming up process. In this work we use a moment closure approach, see e.g. [9] for a short review, which is in terms of accuracy and computational cost a suitable choice, since we decrease the dimensionality and complexity of the problem. The moments are defined by integration w.r.t. the angular variable $\mathbf{\Omega} \in \mathcal{S}^{d-1}$ on the $d-1$- dimensional unit sphere, denoted by $\langle\cdot\rangle$, i.e.,

$$\begin{aligned}E &= \int_{\mathcal{S}^{d-1}} I\,\mathrm{d}\mathbf{\Omega} = \langle I\rangle, \\ \mathbf{F} &= \int_{\mathcal{S}^{d-1}} \mathbf{\Omega} I\,\mathrm{d}\mathbf{\Omega} = \langle \mathbf{\Omega} I\rangle, \\ \mathbf{P} &= \int_{\mathcal{S}^{d-1}} (\mathbf{\Omega}\otimes\mathbf{\Omega}) I\,\mathrm{d}\mathbf{\Omega} = \langle(\mathbf{\Omega}\otimes\mathbf{\Omega})I\rangle,\end{aligned} \tag{6}$$

where d is dimension of the space variable. The 0-th moment E is the radiative energy, $\mathbf{F}$ the radiative flux and $\mathbf{P}$ the pressure tensor. The angular-averaged RTE yields a system of equations which is not closed, since there are too many unknowns, i.e. E, F_x, F_y, F_z and the 6 components of the (symmetric) 3x3 tensor $\mathbf{P}$. There are different approaches for closures. The P_n closure, leading to the spherical harmonics which can be extended to partial moment approximations [30, 8], or the entropy closure leading to the M_n equations [31, 32].

In our model of choice, we use the the P_1 model as it is the classical and most straight-forward closure, see e.g. [8, 9]. It is given by

$$\mathbf{P} = \frac{1}{3}E\,\mathbf{Id}, \tag{7}$$

where $\mathbf{Id}$ is the identity tensor. Using the P_1 closure (7) yields

$$\nabla\cdot\left(\frac{-1}{3(\kappa+\sigma_s)}\nabla E\right) = \kappa(\langle I_b\rangle - E), \tag{8}$$

where the radiative flux is

$$\mathbf{F}^r(E) = \left(\frac{-1}{3(\kappa+\sigma_s)}\nabla E\right). \tag{9}$$

Suitable boundary conditions for moment approximations of the RHTE are a discussed at length in the literature, e.g. [6, 33]. In the following we use boundary conditions for the radiative flux, i.e.,

$$\mathbf{F}^r_\Gamma(E) = \Theta(4\sigma T_w - E), \tag{10}$$

with the wall parameter

$$\Theta = \frac{\epsilon_w}{2(2-\epsilon_w)}, \tag{11}$$

the wall temperature T_w and the wall emissivity ϵ_w. This flux boundary condition is motivated from the work of Sazhin *et al* [34].

2.3 | Heat conduction in solids

We employ Conjugate Heat Transfer in a coupled multiphysics, multizone and AD setting as done in [35, 36]. The governing equation in the solid is given by the heat conduction equation with a disconnected boundary consisting of solid walls S,

$$R(U) = \frac{\partial U}{\partial t} - \nabla \cdot \bar{F}^v(U, \nabla U) - Q = 0,$$
$$T = T_s \quad \text{or} \quad \kappa_s \nabla T \cdot n = q_s, \quad \text{on the boundary,}$$

with the conservative variable $U = \rho_s c_{p_s} T$, whereas ρ_s is the solid density, c_{p_s} is the specific heat of the solid and T is the material temperature. As boundary condition we either impose a Dirichlet condition for the temperature or a Neumann condition for the heat flux with κ_s being the thermal conductivity. The flux takes the following form:

$$\bar{F}^v(U, \nabla U) = \kappa_s \nabla T.$$

As we are not able to estimate a suitable temperature distribution (or a heat flux distribution) at the shared interface of the two zones in advance, the physically correct values are to be found during the simulation, i.e., by coupling energy quantities in both zones which is one of the subjects of the next section.

2.4 | Coupling Conditions

We consider a flow-radiation coupling in zone 1 and the corresponding conjugate heat transfer coupling between zone 1 and zone 2 for the matching material temperature at the shared interface.

1. Zone 1: (Flow - Radiation coupling):
   The coupling of the flow equation $F(\mathbf{q})$ in (4) with the residual RTE $R(E)$ in (12), is approached by segregated fixed point argument, i.e., the governing equations are treated independently and the relevant quantities are exchanged before the start of each inner solver iteration.
   The blackbody intensity in a thermal equilibrium in an absorbing and emitting gray medium is given by Stefan's

law

$$\langle I_b(T)\rangle = 4\sigma T^4, \tag{12}$$

where σ is the Stefan-Boltzmann constant and T is the flow temperature. Hence, we obtain a one-directional coupling from the flow equations into the radiation equations. The coupling from the radiation equations to the flow equations is done using the radiative source term [37]

$$\mathbf{Q}^r(E) = \begin{pmatrix} \cdot \\ \cdot \\ -\nabla \cdot \mathbf{F}^r(E) \end{pmatrix}, \tag{13}$$

and incorporated to the flow equation

$$F(\mathbf{q}, E) = \Gamma(\beta)\frac{\partial \mathbf{q}}{\partial t} + \nabla \cdot \mathbf{F}^c(\mathbf{q}) - \nabla \cdot \mathbf{F}^v(\mathbf{q}) - \mathbf{Q}(\mathbf{q}) - \mathbf{Q}^r(E) = 0. \tag{14}$$

2. Zone 1 - Zone 2 (Conjugate Heat Transfer coupling):
The coupling routine finds a temperature distribution that makes the heat fluxes match on both sides of the interface, i.e., between the zones. The classical approach is to impose the boundary temperature from the solid zone T_s on the adjacent fluid domain directly and relax the resulting heat fluxes until they coincide by setting the heat fluxes from the fluid zone q_f as a (weak) Neumann boundary condition within the solid domain. We consider the combination of conservative variables $U = (U_1, U_2)$, where the subscript index represents the corresponding zone and consider

$$\begin{aligned} &R_1(U_1) = 0 \\ &T = T_s(U_2) \quad \text{at the boundary} \end{aligned}$$

in case R_1 governs the fluid zone and

$$\begin{aligned} &R_2(U_2) = 0 \\ &k_s \nabla T = q_f(U_1) \quad \text{at the boundary} \end{aligned}$$

in case R_2 governs the solid zone.

3 | ADJOINT PROBLEM

The classical approach to compute sensitivities efficiently in optimal control problems is to use adjoint or Lagrange based methods, see e.g. [38] as a classical reference. They have been successfully applied in optimal design problems, such as in phosphate production [3, 4], electric motors [39], fiber optimization [40] and microchannel cooling systems [41].

In Section 3.1 we give a general description of how the shape sensitivities can be derived in the finite dimensional setting. However, even in the discrete setting the application of this method in coupled problems is very complex due

to the requirement of availability of the full, exact problem Jacobian.

An alternative to overcome this problem, that is available in the SU2 context, is to use Algorithmic Differentiation techniques [42, 43] in combination with a fixed point formulation of the problem [15, 16, 20]. This approach is abbreviated as ADDA (AD-based Discrete Adjoint) following the nomenclature in Ref. [20]. The ADDA method for CFD-RHT-CHT problems is presented in Section 3.2 and is the methodology followed in this paper for the computation of gradients.

3.1 | Finite dimensional adjoint approach

We collect the system of governing equations in $g = g(\mathbf{x})$ with $\mathbf{x}$ as state variable, whose solutions solve $g(\mathbf{x}) = 0$. For a given parameter $\boldsymbol{\alpha}$ we done the solution by $\mathbf{x}(\boldsymbol{\alpha})$. Further, let J be a parametrized shape functional.

$$J = J(\mathbf{x}(\boldsymbol{\alpha}), \boldsymbol{\alpha}), \tag{15}$$

where the design variables are given in the vector $\boldsymbol{\alpha}$. The optimal design problem is then summarized via

$$\begin{aligned} &\min_{\boldsymbol{\alpha}} \; J(\mathbf{x}(\boldsymbol{\alpha}), \boldsymbol{\alpha}) \\ &\text{s.t.} \;\; g(\mathbf{x}(\boldsymbol{\alpha}), \boldsymbol{\alpha}) = 0. \end{aligned} \tag{16}$$

The Lagrangian is defined as

$$L = J(\mathbf{x}, \boldsymbol{\alpha}) + \tilde{\mathbf{x}}^T g(\mathbf{x}, \boldsymbol{\alpha}), \tag{17}$$

where the adjoint variable is denoted by $\tilde{\mathbf{x}}$. To get the adjoint equation we differentiate w.r.t to the state variable and calculate

$$\frac{\partial L}{\partial \mathbf{x}} = \frac{\partial J}{\partial \mathbf{x}} + \tilde{\mathbf{x}}^T \frac{\partial g}{\partial \mathbf{x}} = 0, \tag{18}$$

compare e.g. [38]. Using the chain rule for the differentiation of the cost functional with respect to the design parameters yields

$$\frac{\mathrm{d}J}{\mathrm{d}\boldsymbol{\alpha}} = \frac{\partial J}{\partial \boldsymbol{\alpha}} + \frac{\partial J}{\partial \mathbf{x}} \frac{\mathrm{d}\mathbf{x}}{\mathrm{d}\boldsymbol{\alpha}}, \tag{19}$$

and since the derivative vanishes at the optimum additionally

$$\frac{\mathrm{d}g}{\mathrm{d}\boldsymbol{\alpha}} = \frac{\partial g}{\partial \boldsymbol{\alpha}} + \frac{\partial g}{\partial \mathbf{x}} \frac{\mathrm{d}\mathbf{x}}{\mathrm{d}\boldsymbol{\alpha}} = 0. \tag{20}$$

Combining (18), (19) and (20), we get the known formula

$$\frac{\mathrm{d}J}{\mathrm{d}\boldsymbol{\alpha}} = \frac{\partial J}{\partial \boldsymbol{\alpha}} + \tilde{\mathbf{x}}^T \frac{\partial g}{\partial \boldsymbol{\alpha}}. \tag{21}$$

To calculate the derivatives we have to solve for $\tilde{\mathbf{x}}$ by solving the linear system

$$\frac{\partial g}{\partial \mathbf{x}}^T \tilde{\mathbf{x}} = -\frac{\partial J}{\partial \mathbf{x}}^T . \tag{22}$$

The system matrix $\frac{\partial g}{\partial \mathbf{x}}^T$ is the transposed Jacobian of the governing equations.

Hence, by following this approach we need to compute the Jacobian precisely in order to get accurate gradient information, as any simplification in the problem matrix yields an incorrect solution $\tilde{\mathbf{x}}$.

3.2 | Fixed-point adjoint based on Algorithmic Differentiation

We rewrite the governing equations in (16) in the form of a fixed-point iterator, $\mathbf{x} = \mathbf{g}(\mathbf{x})$, which is only feasible at the problem solution,

$$\mathbf{x}^* = \mathbf{g}(\mathbf{x}^*) \iff g(\mathbf{x}^*) = 0. \tag{23}$$

Note, that we are using $\mathbf{g}$ instead of g for the remaining section. The optimization problem results

$$\begin{aligned} &\min_{\boldsymbol{\alpha}} \; J(\mathbf{x}(\boldsymbol{\alpha}), \boldsymbol{\alpha}) \\ &\text{s.t.} \;\; \mathbf{g}(\mathbf{x}(\boldsymbol{\alpha}), \boldsymbol{\alpha}) - \mathbf{x}(\boldsymbol{\alpha}) = 0, \end{aligned} \tag{24}$$

which leads to the problem Lagrangian

$$L = J(\mathbf{x}, \boldsymbol{\alpha}) + \bar{\mathbf{x}}^T \left[\mathbf{g}(\mathbf{x}, \boldsymbol{\alpha}) - \mathbf{x}\right] . \tag{25}$$

Note that we have changed the adjoint variable $\tilde{\mathbf{x}}$ from (17) into $\bar{\mathbf{x}}$, as the current formulation of the problem differs from that in Section 3.1. The adjoint equation that results from (25) is

$$\frac{\partial L}{\partial \mathbf{x}} = \frac{\partial J}{\partial \mathbf{x}} + \bar{\mathbf{x}}^T \frac{\partial \mathbf{g}}{\partial \mathbf{x}} - \bar{\mathbf{x}}^T = 0 \tag{26}$$

and, consequently, we can compute the adjoint variables using a fixed-point equation

$$\bar{\mathbf{x}}^{n+1} = \frac{\partial J}{\partial \mathbf{x}}^T + \frac{\partial \mathbf{g}}{\partial \mathbf{x}}^T \bar{\mathbf{x}}^n, \tag{27}$$

where the matrix-vector product $\frac{\partial \mathbf{g}}{\partial \mathbf{x}}^T \bar{\mathbf{x}}$ will be done using AD.

The operator $\mathbf{g}$ is defined in the computational code as the sequence of operations that are done iteratively to update the state vector,

$$\mathbf{x}^{n+1} = \mathbf{g}(\mathbf{x}^n), \tag{28}$$

for which, at convergence,

$$\mathbf{x}^{n+1} \approx \mathbf{x}^n. \tag{29}$$

In order to solve the adjoint equation (27), the fixed-point operator evaluated at a converged state, $\mathbf{x}^{n+1} = \mathbf{g}(\mathbf{x}^n)$, is recorded by the AD tool CoDiPack. Once the recording is in place, the adjoint vector $\bar{\mathbf{x}}$ is initialized to an initial guess, normally $\bar{\mathbf{x}}^0 = 0$, and the adjoint of the objective functional J is set to $\bar{J} = \mathrm{d}J/\mathrm{d}J = 1.0$. The evaluation of (27) leads to a new solution of the adjoint vector, $\bar{\mathbf{x}}^1$. The iterative process is run until convergence of the adjoint variables $\bar{\mathbf{x}}^n$, and the crossed dependencies are implicitly being considered by recording the transfer of data processes.

It can be shown that the adjoint problem inherits the convergence properties of the primal fixed-point problem [15, 16], i.e., the fixed-point operator $\mathbf{x} = \mathbf{G}(\mathbf{x})$ converges if, according to the Banach fixed-point theorem and in a suitable matrix norm,

$$\left\| \frac{\partial \mathbf{G}}{\partial \mathbf{x}} \right\| < 1. \tag{30}$$

Provided that $\mathbf{G}$ is contractive, so is the recorded adjoint trace. Once the values of the adjoint variables have converged, the gradient of the objective function is directly

$$\frac{\mathrm{d}J}{\mathrm{d}\boldsymbol{\alpha}}^T = \frac{\partial J}{\partial \boldsymbol{\alpha}}^T + \frac{\partial \mathbf{G}}{\partial \boldsymbol{\alpha}}^T \bar{\mathbf{x}}, \tag{31}$$

where the matrix-vector product $\frac{\partial \mathbf{G}}{\partial \boldsymbol{\alpha}}^T \bar{\mathbf{x}}$ can also be computed using AD and an adequate definition of the input variables $\boldsymbol{\alpha}$.

In order to apply this AD-based strategy to a CFD-RHT-CHT problem, attention has to be paid to the presence of two segregated primal fixed point iterators, $\mathbf{G}_{\text{CFD-RHT}}$ and $\mathbf{G}_{\text{S}}$, instead of a single $\mathbf{G}$.
Defining $x := (x_{\text{F}}, x_{\text{S}})$ as the combined vector of fluid state variables ($x_{\text{F}} := (\mathbf{q}, E)$) and the solid state variable (x_{S}, temperature in our configuration), and $\mathbf{G} := (\mathbf{G}_{\text{CFD-RHT}}, \mathbf{G}_{\text{S}})$ as the combined vector of both iterator outputs, the adjoint fixed-point iteration equation (27) turns into

$$\begin{pmatrix} \bar{\mathbf{x}}_{\text{F}}^{n+1} \\ \bar{\mathbf{x}}_{\text{S}}^{n+1} \end{pmatrix} = \begin{pmatrix} \frac{\partial J}{\partial x_{\text{F}}} \\ \frac{\partial J}{\partial x_{\text{S}}} \end{pmatrix} + \begin{pmatrix} \frac{\partial \mathbf{G}^{\text{CFD-RHT}}}{\partial x_{\text{F}}} & \frac{\partial \mathbf{G}^{\text{CFD-RHT}}}{\partial x_{\text{S}}} \\ \frac{\partial \mathbf{G}^{\text{S}}}{\partial x_{\text{F}}} & \frac{\partial \mathbf{G}^{\text{S}}}{\partial x_{\text{S}}} \end{pmatrix}^T \begin{pmatrix} \bar{\mathbf{x}}_{\text{F}}^{n} \\ \bar{\mathbf{x}}_{\text{S}}^{n} \end{pmatrix}, \tag{32}$$

which can be solved by using the discrete adjoint functionality for multiphysics in SU2 [36].
Note that SU2 generates and evaluates each block in (32) in a black-box manner which implies that cross dependencies between coupled solvers within one iterator (e.g. the flow and radiation solver) will be automatically resolved in each adjoint evaluation process. Adjoint contributions resulting cross dependencies between iterators (colored blue) are, however, extracted and stored in separated data structures. For our application, they have a intuitive physical interpretation:

- $\partial \mathbf{G}^{\text{CFD-RHT}}/\partial x_{\text{S}}$ constitutes the CFD-RHT solver's dependence on the temperature of the solid, this is due to the temperature at the interface which determines the heat flux;
- $\partial \mathbf{G}^{\text{S}}/\partial x_{\text{F}}$ represents the heat solver's dependence on the heat fluxes at the interface, which are determined by the CFD-RHT solver.

Their explicit handling also allows for better control of repeated inner (i.e. zone-wise) and outer updates that involve the update of cross derivatives. For further details, especially how this can be done in an efficient way, we refer to [36].

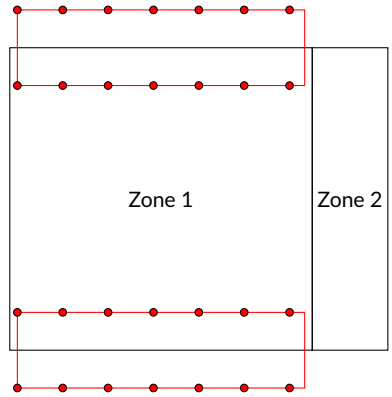

FIGURE 2 FFD Boxes (red) that allow the deformation of the upper and lower part of the flow domain.

Having obtained the fixed-point solution $(\bar{\mathbf{x}}_F^*, \bar{\mathbf{x}}_S^*)$ to (32), sensitivities of the objective function J with respect to design parameters α (that might be defined for the fluid and the solid zone, e.g. think of α as mesh coordinates) can be as normal derived by

$$\frac{\mathrm{d}J}{\mathrm{d}\alpha}^T = \frac{\partial L}{\partial \alpha}^T = \frac{\partial J}{\partial \alpha}^T + \frac{\partial \mathbf{G}}{\partial \alpha}^T \begin{pmatrix} \bar{\mathbf{x}}_F^* \\ \bar{\mathbf{x}}_S^* \end{pmatrix} \tag{33}$$

where $\frac{\partial \mathbf{G}}{\partial \alpha}$ is the vector with derivatives of both fixed-point iterators with respect to α.

4 | NUMERICAL RESULTS

The code being used throughout this section can be accessed on GitHub: `https://github.com/NicoDietrich/Tutorials/blob/feature_radiation_multizone/README.md`. It is tested with SU2 v7.0.6. We partition the domain into two sub-domains, as can be seen in Figure 1. As a benchmark problem we solve the turbulent buoyancy-driven cavity coupled with a conjugate heat transfer interaction towards the solid. The numerical setting and the configuration files to solve the primal and adjoint equations are explained in depth in a SU2 Tutorial, `https://su2code.github.io/tutorials/Turbulent_RHT_CHT/`.

We discretize the flow domain with 4800 elements and the solid domain with 960 elements, both in a structured mesh. To allow the deformation of the upper and lower part of the domain we define the respective FFD boxes to almost touch the boundary of the flow domain which results in a total of 28 design variables parameterizing the domain, i.e. 14 for the upper boundary FFD box and 14 for the lower boundary FFD box. To ensure a smooth transition of the boundary from zone 1 to zone 2 we prescribe a second order condition and hence fix $2 \cdot 2$ degrees of freedom. This results in 24 design parameters. In Section 4.1 we verify the computed sensitivities by comparing it to a central difference approximation of the shape sensitivity. In Section 4.2 a gradient descent algorithm is applied to test the performance of the calculated sensitivities.

4.1 | Adjoint sensitivities verification

In order to ensure the correctness of our proposed methodology, we verify $\nabla J_{adj} = \frac{\mathrm{d}J}{\mathrm{d}\boldsymbol{\alpha}}^T$ using a central different approximation. For that we perturb the i-th design parameter into the the scaled unit direction e_i, calculate the central difference quotient

$$\nabla J_h^i = \frac{J(\mathbf{x}(\boldsymbol{\alpha}_0 + he_i), \boldsymbol{\alpha}_0 + he_i) - J(\mathbf{x}(\boldsymbol{\alpha}_0 - he_i), \boldsymbol{\alpha}_0 - he_i)}{2h}, \tag{34}$$

and compare it to ∇J_{adj}^i in the euclidean distance for the different scales $h \in \{10^{-3}, 10^{-4}, 10^{-5}, 10^{-6}, 10^{-7}\}$. The normalized results for $\boldsymbol{\alpha}_0 = 0$ are shown in Figure 3. We see a significant increase in accuracy from $h = 0.001$ to $h = 0.0001$ and an artifact of numerical errors for $h = 10^{-7}$. For the choices of h in between the approximation indicates sufficient accuracy of the adjoint sensitivities. To check the accuracy of the sensitivities during an optimization loop a second verification is done on an already displaced initial domain, given by

$$\begin{aligned}\boldsymbol{\alpha}_1 = [&0.0, 0.05, 0.1, 0.14, 0.16, 0.17, 0.175, 0.17, 0.16, 0.14, 0.1, 0.05,\\ &0.0, -0.05, -0.1, -0.14, -0.16, -0.17, -0.175, -0.17, -0.16, -0.14, -0.1, -0.05].\end{aligned}$$

Computing the central difference on this domain results in a lower accuracy compared to no initial displacement but the results verify the adjoint gradient to a sufficient degree, see Figure 3.

4.2 | Shape Optimization

The verification in Section 4.1 that $\nabla J_{adj} = \frac{\mathrm{d}J}{\mathrm{d}\boldsymbol{\alpha}}^T$ is a sufficiently good approximation of the gradient of the reduced cost functional, enables us to use this gradient information in a steepest descent method. As a stepsize displacement control method we use an Armijo type rule. In the first iteration we set the initial design vector $\boldsymbol{\alpha}_0 = 0$ and use the gradient $\nabla J_{adj}(\boldsymbol{\alpha}_0)$ and the directional derivative into gradient direction $\nabla J_{adj}(\boldsymbol{\alpha})^T \nabla J_{adj}(\boldsymbol{\alpha}) = \|\nabla J_{adj}(\boldsymbol{\alpha})\|$ to check if

$$\hat{J}(\boldsymbol{\alpha}_0) - \hat{J}(\boldsymbol{\alpha}_0 + \gamma \nabla J_{adj}) < \sigma\gamma \|\nabla J_{adj}(\boldsymbol{\alpha})\| = tol, \tag{35}$$

where $\hat{J}(\boldsymbol{\alpha}) = J(\mathbf{x}(\boldsymbol{\alpha}), \boldsymbol{\alpha})$ and the gradient direction is scaled with $\gamma = \gamma_0 \hat{\gamma} \cdot \frac{1}{\|s\|_{l2}}$, i.e, we normalize the gradient and scale the chosen initial stepsize γ_0 and $\sigma = 10^{-4}$ is the typical choice given in the literature. We check Condition 35 for $\hat{\gamma} \in \{1, \frac{1}{2}, \frac{1}{4}, \dots\}$ until we find $\hat{\gamma}^*$ which satisfies the condition and update $\boldsymbol{\alpha}_1 = \boldsymbol{\alpha}_0 + \gamma \nabla J_{adj}$. However, since solving the state and adjoint equations proved to be challenging, especially on perturbed domains, we deviate from the usual implementation by not accepting $\hat{\gamma}^*$ right away. Instead we only continue if state and adjoint solvers converge on this perturbed domain and look for another $\hat{\gamma}$ and therefore $\boldsymbol{\alpha}_1$ otherwise. Doing the procedure on domains which were already displaced, e.g., $0 < i \rightarrow i + 1$ one has to pay attention to the following detail: because the adjoint based sensitivities s_{i+1} provided by SU2 are always relative to the initial domain we have to substract the previous deformation to get the actual gradient, i.e., $\nabla J_{adj_1}(\boldsymbol{\alpha}) = s_{i+1} - \boldsymbol{\alpha}_i$. Using the actual gradient one can proceed as described before.

Using this method we observe a main feature: Defining the FFD box in a way such that it does not include the upper left mesh point is critical, as doing so results in a broken mesh because the optimizer expands the left boundary without distributing the perturbation onto the boundary mesh. The resulting elements are hence too large and thus

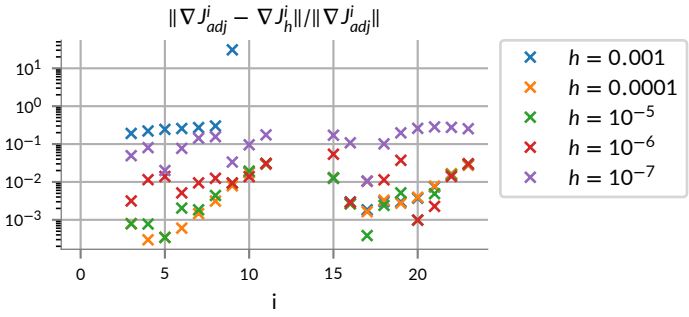

(a) Computation done on the initial domain.

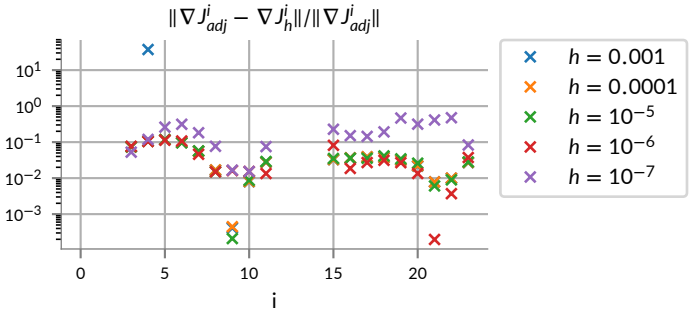

(b) Computation done on the perturbed domain.

FIGURE 3 Relative Euclidean distance between finite difference approximation of the shape sensitivities (∇J_h) and the sensitivities obtained by the proposed methodology (∇^i_{adj}), for different stepsizes h, the degrees of freedom are numbered with i. For $i = 1, 2, 3, 12, 13, 14$ the gradient is zero which is exactly replicated by the adjoint based gradient.

decrease drastically the mesh quality on which the approximation on the primal and adjoint problem are unreliable. An example of such a deformation is displayed in Figure 5.

Figure 6 and Figure 7 show the initial and optimized shapes in both test cases with corresponding state solutions. The increase of about 4% in the objective functional in the first test case, can be seen in Figure 5a. Starting from different initial shapes, the proposed optimization yields similar optimized shapes, i.e., a similar stationary point, see the comparison in Figure 8.

5 | CONCLUSION

We presented a benchmark problem to an applied industrial shape design optimization problem which we treated with a novel approach to compute adjoint sensitivities in a multiphysics framework. We justified this methodology by a finite difference approach and demonstrated its feasibility by optimizing two different test cases. These promising results motivate further research in multidisciplinary and multizone shape optimization problems based on discrete adjoint methods in SU2 and potentially more application to real world high temperature processes apart from phosphate production.

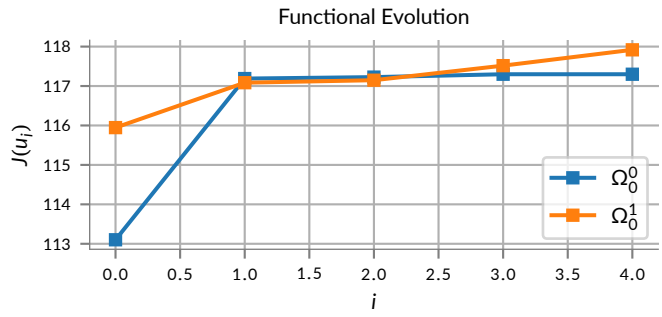

FIGURE 4 For both initial domains the functional value increases significantly. Here, Ω_0^0 denotes the unperturbed and Ω_0^1 the perturbed initial domain.

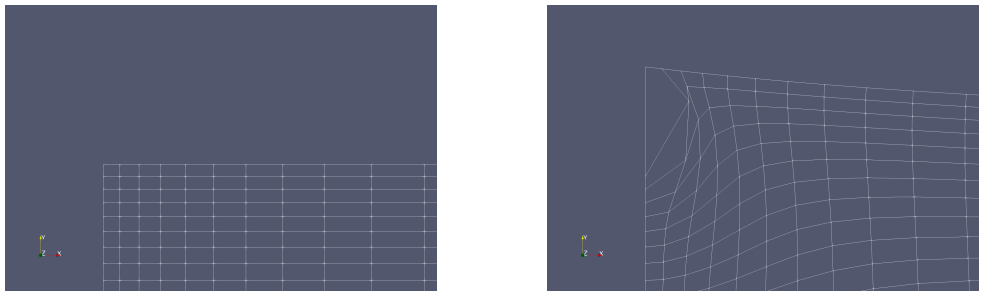

(a) Initial mesh

(b) "Final mesh"

FIGURE 5 Mesh deformation with FFD box including the upper left mesh point

Acknowledgements

This project has been supported by the German Federal Ministry of Education and Research (BMBF) under grant number 05M18UKA.

references

[1] Seaid M, Klar A, Pinnau R. Numerical Solvers for Radiation and Conduction in High Temperature Gas Flows. FLOW TURBUL COMBUST 2005;75:173–190.

[2] Seaid M, Frank M, Klar A, Pinnau R, Thömmes G. Efficient numerical methods for radiation in gas turbines. J COMPUT APPL MATH 2004;170(1):217 – 239.

[3] Marx T, Dietrich N, Pinnau R. Shape Optimization in High Temperature Processes. PAMM 2019;.

[4] Dietrich N, Marx T, Pinnau R. Shape Optimization in Phosphate Production. PAMM 2019;.

[5] Pinnau R, Thömmes G. Optimal boundary control of glass cooling processes. MATH METHOD APPL SCI 2004;27:1261 – 1281.

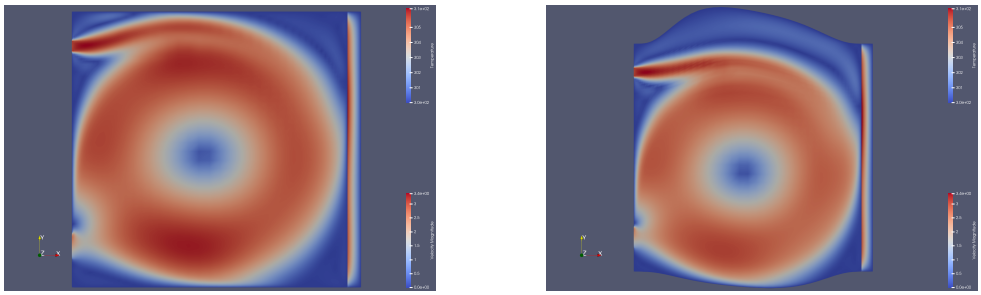

(a) Initial solution. (b) Final solution.

FIGURE 6 Optimization with FFD box excluding the upper left mesh point

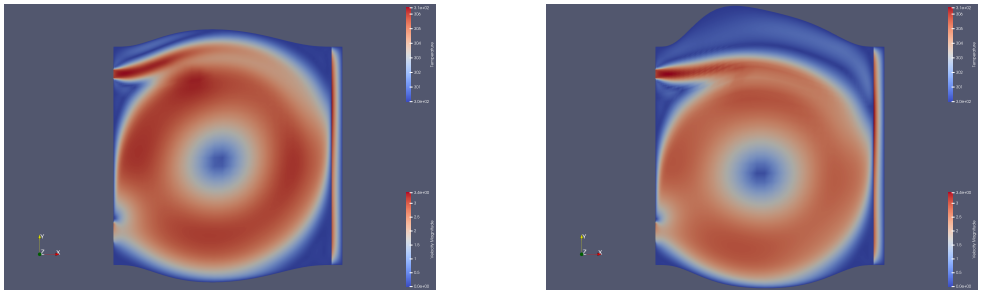

(a) Initial solution. (b) Solution.

FIGURE 7 Optimization with FFD box excluding the upper left mesh point using a different initial geometry

[6] Modest MF, Yang J. Elliptic PDE formulation and boundary conditions of the spherical harmonics method of arbitrary order for general three-dimensional geometries. Journal of Quantitative Spectroscopy and Radiative Transfer 2008 jun;109(9):1641–1666.

[7] Case KM, Zweifel PF. Linear Transport Theory. Addison-Wesley series in nuclear engineering, Addison-Wesley Publishing Company; 1967. https://books.google.de/books?id=JZE8AAAAIAAJ.

[8] Frank M, Dubroca B, Klar A. Partial moment entropy approximation to radiative heat transfer. Journal of Computational Physics 2006 oct;218(1):1–18.

[9] Frank M. Approximate models for radiative transfer. Bulletin of the Institute of Mathematics Academia Sinica New Series 2007 01;2.

[10] Pinnau R, Siedow N. Optimization and Inverse Problems in Radiative Heat Transfer. In: Constrained Optimization and Optimal Control for Partial Differential Equations Springer Basel; 2011.p. 597–609.

[11] Pinnau R, Tse O. Optimal control of a simplified natural convection-radiation model. Communications in Mathematical Sciences 2013;11(3):679–707.

[12] Kenway GKW, Kennedy GJ, Martins JRRA. Scalable Parallel Approach for High-Fidelity Steady-State Aeroelastic Analysis and Adjoint Derivative Computations. AIAA Journal 2014 may;52(5):935–951.

[13] Palacios F, Economon TD, Wendorff AD, Alonso JJ. Large-scale aircraft design using SU2. In: 53rd AIAA Aerospace Sciences Meeting; 2015. .

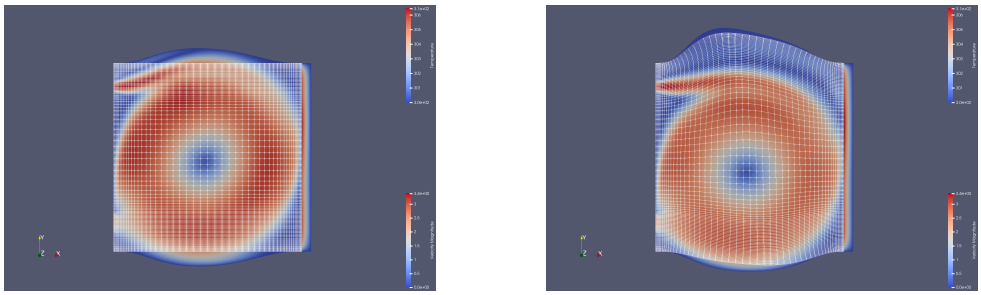

(a) Initial shape/solution.

(b) Final shape/solution.

FIGURE 8 Comparison of optimization using different initial shapes. The initial and optimized state starting from the perturbed domain are in the background and the initial and optimized mesh of the optimization starting at the original initial shape in the foreground.

[14] Abu-Zurayk M. An Aeroelastic Coupled Adjoint Approach for Multi-Point Designs in Viscous Flows. PhD thesis, RWTH Aachen University; 2016.

[15] Albring TA, Sagebaum M, Gauger NR. Development of a Consistent Discrete Adjoint Solver in an Evolving Aerodynamic Design Framework. In: 16th AIAA/ISSMO Multidisciplinary Analysis and Optimization Conference American Institute of Aeronautics and Astronautics; 2015. .

[16] Albring TA, Sagebaum M, Gauger NR. Efficient Aerodynamic Design using the Discrete Adjoint Method in SU2. In: 17th AIAA/ISSMO Multidisciplinary Analysis and Optimization Conference American Institute of Aeronautics and Astronautics; 2016. .

[17] Zhou BY, Albring TA, Gauger NR, Economon TD, Palacios F, Alonso JJ. A Discrete Adjoint Framework for Unsteady Aerodynamic and Aeroacoustic Optimization. In: 16th AIAA/ISSMO Multidisciplinary Analysis and Optimization Conference American Institute of Aeronautics and Astronautics; 2015. .

[18] Zhou B, Albring TA, Gauger NR, Ilario C, Economon TD, Alonso JJ. Reduction of Airframe Noise Components Using a Discrete Adjoint Approach. In: 18th AIAA/ISSMO Multidisciplinary Analysis and Optimization Conference American Institute of Aeronautics and Astronautics; 2017. .

[19] Economon T. Simulation and Adjoint-based Design for Variable Density Incompressible Flows with Heat Transfer. In: 2018 Multidisciplinary Analysis and Opt. Conference American Institute of Aeronautics and Astronautics; 2018. .

[20] Sanchez R, Albring T, Palacios R, Gauger NR, Economon TD, Alonso JJ. Coupled adjoint-based sensitivities in large-displacement fluid-structure interaction using algorithmic differentiation. International Journal for Numerical Methods in Engineering 2017 nov;113(7):1081–1107.

[21] Sanchez R. A coupled adjoint method for optimal design in fluid-structure interaction problems with large displacements. PhD thesis, Imperial College London; 2018.

[22] Palacios F, Colonno MR, Aranake AC, Campos A, Copeland SR, Economon TD, et al. Stanford University Unstructured (SU2): An open-source integrated computational environment for multi-physics simulation and design. In: AIAA 51st Aerospace Sciences Meeting, 7-10 January Grapevine, TX; 2013. .

[23] Palacios F, Economon TD, Aranake AC, Copeland SR, Lonkar AK, Lukaczyk TW, et al. Stanford university unstructured (SU2): Open-source analysis and design technology for turbulent flows. In: AIAA 52nd Aerospace Sciences Meeting, SciTech, 13-17 January National Harbor, MD; 2014. .

[24] Economon TD, Palacios F, Copeland SR, Lukaczyk TW, Alonso JJ. SU2: An open-source suite for multiphysics simulation and design. AIAA Journal 2016;54(3):828–846.

[25] Chai JC, Lee HS, Patankar SV. Finite volume method for radiation heat transfer. Journal of Thermophysics and Heat Transfer 1994 jul;8(3):419–425.

[26] Koch R, Krebs W, Wittig S, Viskanta R. Discrete ordinates quadrature schemes for multidimensional radiative transfer. Journal of Quantitative Spectroscopy and Radiative Transfer 1995 apr;53(4):353–372.

[27] Murthy JY, Mathur SR. Finite Volume Method for Radiative Heat Transfer Using Unstructured Meshes. Journal of Thermophysics and Heat Transfer 1998 jul;12(3):313–321.

[28] Man Young Kim J Seung Wook Baek. UNSTRUCTURED FINITE-VOLUME METHOD FOR RADIATIVE HEAT TRANSFER IN A COMPLEX TWO-DIMENSIONAL GEOMETRY WITH OBSTACLES. Numerical Heat Transfer, Part B: Fundamentals 2001 jun;39(6):617–635.

[29] Joseph D, Hafi ME, Fournier R, Cuenot B. Comparison of three spatial differencing schemes in discrete ordinates method using three-dimensional unstructured meshes. International Journal of Thermal Sciences 2005 sep;44(9):851–864.

[30] Dubroca B, Klar A. Half-Moment Closure for Radiative Transfer Equations. Journal of Computational Physics 2002 aug;180(2):584–596.

[31] Ripoll JF, Dubroca B, Audit E. A FACTORED OPERATOR METHOD FOR SOLVING COUPLED RADIATION-HYDRODYNAMICS MODELS. Transport Theory and Statistical Physics 2002 jan;31(4-6):531–557.

[32] Kanno Y, Harada T, Hanawa T. Kinetic Scheme for Solving the M1 Model of Radiative Transfer. Publications of the Astronomical Society of Japan 2013 aug;65(4):72.

[33] Larsen EW, Thömmes G, Klar A, Seaïd M, Götz T. Simplified P_N Approximations to the Equations of Radiative Heat Transfer and Applications. Journal of Computational Physics 2002;183:652–675.

[34] Sazhin SS, Sazhina EM, Faltsi-Saravelou O, Wild P. The p-1 model for thermal radiation transfer: Advantages and limitations. Fuel 1996;75(3):289–294.

[35] Burghardt O, Gauger NR, Economon TD. In: Coupled Adjoints for Conjugate Heat Transfer in Variable Density Incompressible Flows;. https://arc.aiaa.org/doi/abs/10.2514/6.2019-3668.

[36] Burghardt O, Gauger NR, Gomes P, Palacios R, Kattmann T, Economon TD. In: Coupled Discrete Adjoints for Multiphysics in SU2;. https://arc.aiaa.org/doi/abs/10.2514/6.2020-3139.

[37] Jensen K, Ripoll J, Wray A, Joseph D, Elhafi M. On various modeling approaches to radiative heat transfer in pool fires. Combustion and Flame 2007 mar;148(4):263–279.

[38] Hinze M, Pinnau R, Ulbrich M, Ulbrich S. Optimization with PDE Constraints. Mathematical modelling–theory and applications, Springer Netherlands; 2009. https://books.google.de/books?id=GCnJxgEACAAJ.

[39] Gangl P, Langer U, Laurain A, Meftahi H, Sturm K. Shape Optimization of an Electric Motor Subject to Nonlinear Magnetostatics. SIAM Journal on Scientific Computing 2015;37(6):B1002–B1025. https://doi.org/10.1137/15100477X.

[40] Hohmann R, Leithäuser C. Shape Optimization of a Polymer Distributor Using an Eulerian Residence Time Model. SIAM Journal on Scientific Computing 2019;41(4):B625–B648. https://doi.org/10.1137/18M1225847.

[41] Blauth S, Leithäuser C, Pinnau R. Model Hierarchy for the Shape Optimization of a Microchannel Cooling System. arXiv 2019;.

[42] Fateman RJ. Automatic Differentiation of Algorithms: Theory, Implementation, and Application (Andreas Griewank and George F. Corliss, eds.). SIAM Review 1993 dec;35(4):659–660.

[43] Andreas Griewank AW. Evaluating Derivatives: Principles and Techniques of Algorithmic Differentiation. CAMBRIDGE UNIV PR; 2008.